

## Article

# Analytical and 3D Numerical Study of Multilayer Shielding Effectiveness for Board Level Shielding Optimization

Roman Leduc <sup>1</sup>, Njomza Ibrahim <sup>1</sup>, Jean-Marc Dienot <sup>1,2</sup>, Veronika Gavrilenko <sup>1</sup> and Robert Ruscassié <sup>1,\*</sup>

<sup>1</sup> Laboratory for Applied Mechanical and Electrical Engineering Sciences—IPRA Federation, University of Pau et des Pays de l'Adour/E2S UPPA, 64000 Pau, France

<sup>2</sup> SIAME-Labceem, University Paul Sabatier—Toulouse III, 31062 Tarbes, France

\* Correspondence: robert.ruscassie@univ-pau.fr

**Abstract:** The strong development of solid-state power sources offers numerous benefits (such as higher operating frequencies and reduced switching times and power losses), but contributes inherently to the extended range of electromagnetic interferences (EMI). As these systems are associated with a set of embedded monitoring devices using low amplitude signals, it becomes necessary to consider new critical cases of electromagnetic (EM) immunity correlated to such environments. The most common solution against aggressive radiated EMI is the metallic enclosure, which brings a strong shielding effectiveness (SE), but is it always the best compromise? Our study in this paper is focused on the SE of multilayer designs and is therefore intended to optimize the enclosures' compactness for board level shielding (BLS) on printed circuit boards (PCB). First, results are presented, based on metallic multilayer shielding theory and parametric numerical studies in the intentional electromagnetic interferences (IEMI) frequency range, from 0.2 to 5 GHz. Then, a complete 3D EM co-simulation model using the microwave and design modules of CST Studio Suite (which includes the subject, the EMI radiating source, and the multilayer shielding) is proposed, with emphasis on the pertinent choices regarding layers width and their arrangement for compact EM shielding and immunity optimization.

**Keywords:** electromagnetics interferences (EMI); intentional electromagnetic interferences (IEMI); shielding; multilayer; radiated immunity



**Citation:** Leduc, R.; Ibrahim, N.; Dienot, J.-M.; Gavrilenko, V.; Ruscassié, R. Analytical and 3D Numerical Study of Multilayer Shielding Effectiveness for Board Level Shielding Optimization. *Electronics* **2022**, *11*, 4156. <https://doi.org/10.3390/electronics11244156>

Academic Editor: Dah-Jye Lee

Received: 7 November 2022

Accepted: 11 December 2022

Published: 13 December 2022

**Publisher's Note:** MDPI stays neutral with regard to jurisdictional claims in published maps and institutional affiliations.



**Copyright:** © 2022 by the authors. Licensee MDPI, Basel, Switzerland. This article is an open access article distributed under the terms and conditions of the Creative Commons Attribution (CC BY) license (<https://creativecommons.org/licenses/by/4.0/>).

## 1. Introduction

Electromagnetic interference (EMI) is an inherent phenomenon in the world of electrical pulsed power technologies and goes along with the recent technological progress regarding their associated monitoring devices [1,2]. Pulsed power (PP) generators more and more often feature solid-state devices and, more specifically, wide-bandgap semiconductors. This technology trends to replace spark gap switches by offering an equivalent power range and an increased pulse repetition frequency [3,4]. EMI produced by such generators can be classified as intentional electromagnetic interferences (IEMI) [5], the frequency of which is expected to extend from 200 MHz to 5 GHz (see depiction in Figure 1). Additionally, unintentional sources (including solid-state devices used for new applications, such as solar inverters [6], high-speed electric motor supply [7], thermal heating [8], etc.) will bring considerable EMI due to their high frequency (HF) transient current and voltage shapes, corresponding to the same frequency range as IEMI.

PP sources or HF application systems are both designed with necessary core components to fulfill their role, and often come equipped with a set of monitoring devices—e.g., analog to digital converters (ADC)—to be able to survey and detect electrical and physical behaviors. However, the actual improvements in processing speed, component size compactness, or operating voltages reduction of these monitoring systems turn them into significant targets for EMI issues in such harsh EM environments [9]. Therefore, it is essential nowadays to consider

EM immunity during the design process by trying to comply with both low couplings and protection rules.

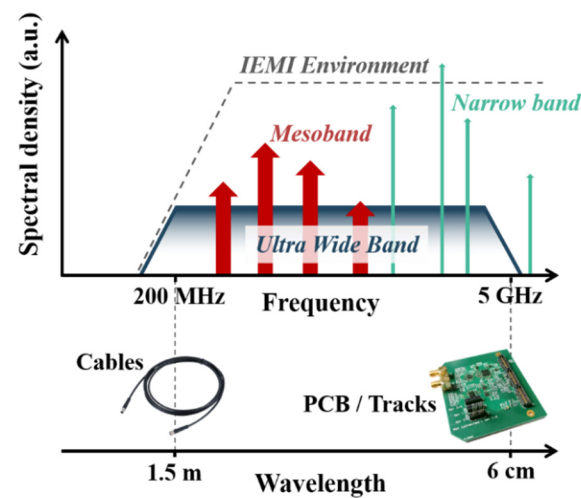


**Figure 1.** Relationship between the IEMI frequency range and its equivalent wavelength range in accordance with potential target's scale.

Among the EMI protection solutions, the most straightforward one is the shielding based on metallic enclosures [10,11]. Shielding technics can be adapted and selected either in cases of far field or near field illumination, depending on where a subject is in the aggressive environment [12,13]. Different examples and solutions proposed by [14,15] provide good knowledge in estimating the shielding effectiveness (SE) of simple metallic screens or enclosures. However, these solutions may appear bulky for embedded systems, or unadaptable for applications requiring low volume and weight constraints. Recent shielding designs based on a multilayer arrangement [16–18], which have drawn our interest in answering this issue, will be the focus of our study. Within our previous work, we developed a high-speed 250 MS/s ADC board based on FPGA-SoC technology to monitor a set of data in an embedded and real-time environment [19]. This device can perform high frequency data acquisition and multiplexed data transmission and must be able to operate in harsh environments, as presented in Figure 2.

This system represents a proper example since it is essential to ensure data and signal integrity on the ADC board, which is the most EMI-exposed part of the system. Our main goal here is to propose new EMI protection shielding designs optimized by means of analytical and 3D numerical models. The proposed shielding configurations contribute to minimizing detrimental EMI impacts on the ADC board, it being a highly embedded feature.

In Part II, we present a state-of-the-art study focused on theoretical single layer and multilayer shielding technics which are based on the transmission line model. In Part III, we compare results obtained from analytical and numerical models. The shielding materials are proposed basing on very thin metallic and insulating materials (10–100  $\mu\text{m}$ ). The parametric numerical studies based on infinitely plane screens gave us good guidance to propose new optimized shielding solutions dedicated to our target configuration (ADC board). Part IV shows the impact of our proposed shielding solutions on the susceptibility and the immunity of the target. For this, we describe a complete 3D numerical model developed, including the IEMI Source (Antenna) and the subject (PCB). Finally, conclusions on the advantages of multilayer shielding designs over the single-layer ones are enounced. Application of this work to new embedded target configurations is discussed.

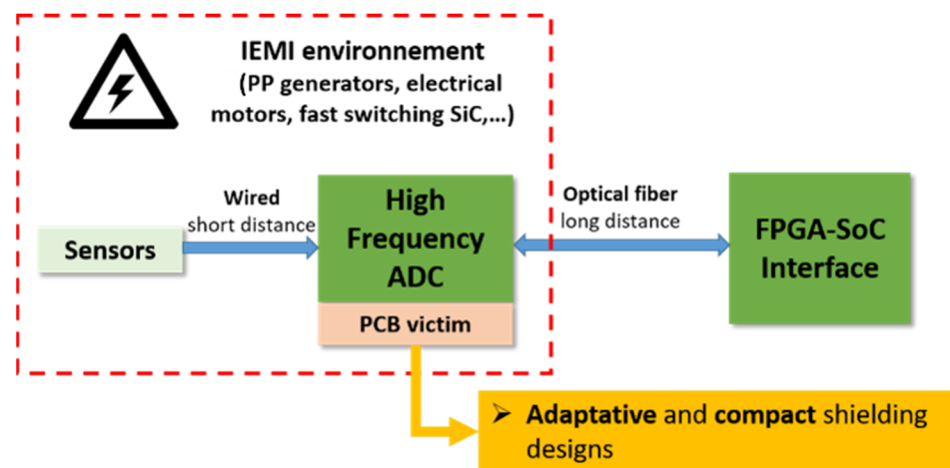


**Figure 2.** Synoptic diagram of the functional and EM environment of the monitoring system based on FPGA-SoC technology.

## 2. Theoretical Analysis of Multilayer Shielding Screens

The shielding effectiveness of an enclosure or a screen is characterized by its ability to isolate an environment from any potentially disturbing EM source. It can be seen either as a protection of an electronic device (subject) or as an attenuation of its radiated emissions (source). Three approaches can be used for the evaluation of the SE variations as a function of the frequency: analytical calculations derived from theoretical models of simplified structures (1D, 2D), numerical calculations on complex and accurate 3D models, or SE experimental measurements technics using specific HF equipment (high power sources, HF receivers). The accuracy estimation of each of these methods is a complex challenge, which is strongly dependent on the relevance of the analytical model, the numerical solver, and the experimental setup. Therefore, it is important to involve at least two methods in the study, such as numerical and analytical approaches, to ensure the validity of the obtained results. Obtaining experimental SE measurements is inherently difficult, especially with high shielding levels, as will be discussed in the following sections. The analytical model used for this study is based on the transmission line theory. This model is first introduced for a single metallic screen. Then, based on [20], the model has been adapted to provide an accurate calculation for multilayer shielding screens.

### 2.1. Analytical Study of a Single Metallic Sheet

The shielding effectiveness SE of a metallic shielding at a given point (see Figure 3) is determined as the ratio of the measured field strength (electric field  $E$  or magnetic field  $H$ ) without and with shielding:

$$SE = 20 \log_{10} \frac{\text{Field without shielding}}{\text{Field with shielding}} \quad (1)$$

where SE is expressed in dB,  $E$  in V/m, and  $H$  in A/m.

SE leans on three well-known mechanisms that can be described by the following representative expressions [10]: the reflection efficiency  $R$ , the absorption efficiency  $A$ , and the multiple reflection losses  $M$ . All of them are expressed in dB; however it should be noted that  $M$  has a negative value, meaning that the latter decreases the shielding effectiveness. The global value of SE is obtained by summing these coefficients:

$$SE = R + A + M. \quad (2)$$

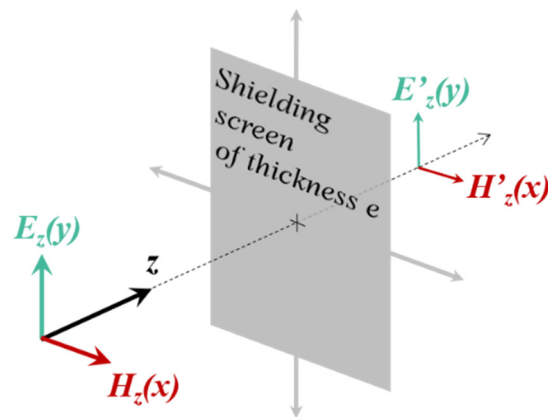


Figure 3. Shielding screen damping incident EM field.

Supposing that an infinite metallic plane is placed in air orthogonally to the incident EM field propagation direction (see Figure 3), the mismatch impedance between air and metallic screen will induce EM reflection. The reflection efficiency  $R$  can be expressed as:

$$R = 20 \log_{10} \left| \frac{(Z_0 + Z_s)^2}{4Z_0Z_s} \right| \tag{3}$$

where  $Z_0$  is the EM wave impedance in air and  $Z_s$  is the metallic plane impedance. In far field, or at a sufficient distance  $d > \lambda/2\pi$  from an EM field impedance point of view (with  $\lambda$  being the wavelength of the EM field),  $E$ -field and  $H$ -field can be considered as coupled, resulting in the impedance value  $Z_0 \approx 377 \Omega$ . In near field, the impedance depends on the type of field source and on frequency,  $Z_E = 1/\omega\epsilon_0d$  or  $Z_H = \omega\mu_0d$ , with  $\omega$  being the angular frequency of the  $E$ -field or  $H$ -field,  $\epsilon_0$  being the vacuum dielectric permittivity and  $\mu_0$  being the vacuum magnetic permeability.

The metallic screen impedance  $Z_s$  depends on its thickness  $e$  and on the skin depth  $\delta$ . If  $e < 0.7\delta$ , only the surface resistance of the screen  $R_s$  is considered (see Equation (4)), and the latter does not depend on the frequency. Otherwise, the intrinsic impedance  $Z_i$  is dominant and then independent from the screen thickness [21].

$$R_s = \frac{1}{\sigma_e} \quad (e < 0.7\delta) \tag{4}$$

$$Z_i = \sqrt{\frac{j\omega\mu_e}{\sigma_e + j\omega\epsilon_e}} \approx \sqrt{\frac{j\omega\mu_e}{\sigma_e}} \quad (e > 0.7\delta) \tag{5}$$

where  $\sigma_e$ ,  $\epsilon_e$ , and  $\mu_e$ , are the conductivity, the dielectric permittivity, and the magnetic permeability of the metallic screen, respectively. Considering  $\sigma_e \gg \epsilon_e$ , the parameter  $\epsilon_e$  is neglected as also seen from Equation (10).

The absorption losses are related to the skin depth and the EM field capability to penetrate the conductor. Consequently, its corresponding contribution to the SE is given by:

$$A = 20 \log_{10} \left[ \exp\left(\frac{e}{\delta}\right) \right]. \tag{6}$$

The multiple reflections are internal since they occur inside the screen. Considering the shielding plane as a transmission line of a length  $x = e$ , the absorbed EM wave is reflected towards the opposite side of the line each time it reaches the boundary, at either  $x = 0$  or  $x = e$ , thus transmitting a slight amount of the incident EM field strength outside the

screen. In this case, the ratio between the amount of energy transmitted outside and the total energy initially supplied into the screen for a good conductor given in dB will be

$$M = 20 \log_{10} \left( 1 - \Gamma_{x=0} \Gamma_{x=e} \exp \left( -\frac{2e}{\delta} \right) \right) \tag{7}$$

where  $\Gamma_{x=0}$  and  $\Gamma_{x=e}$  are the reflection coefficients at each boundary [21]. As the EM field hardly penetrates metallic enclosures at high frequencies, the losses  $M$  are commonly neglected. However, in the case of very thin conducting films of a few micrometers in thickness, the thickness can be close to  $\delta$ , leading to a more significant value of losses  $M$ .

### 2.2. Analytical Model of Multilayer Shielding Screens

To maximize the reflection efficiency, we now study multilayer screen designs that are based on  $N$  conductive layers alternately disposed in between insulating layers (see Figure 4). The transmission line model can be applied to a layer stack (with various properties) in the same way it was used before to calculate the single layer shielding screen  $SE$ . The total  $SE$  of a multilayer screen is the sum of the  $SE$  of each layer. It should be noted that since insulating layers have very low conductivity ( $\sigma \approx 0$ ), their reflection and absorption efficiencies are equal to zero:

$$SE_M = SE_1 + SE_2 + \dots + SE_N . \tag{8}$$

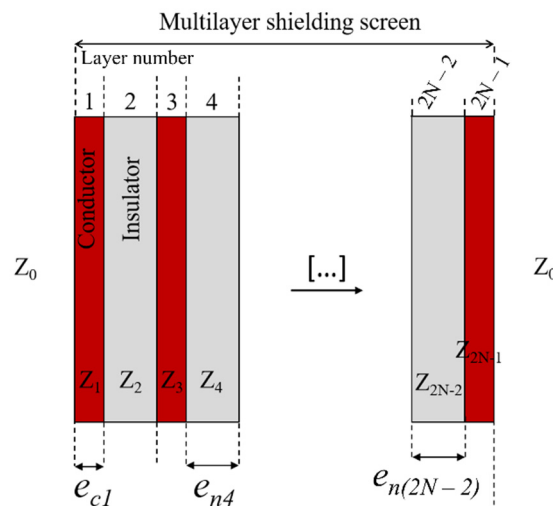


Figure 4. Multilayer shielding with  $N$  conducting layers separated by insulating layers.

Based on [20], the  $M_n$  losses for an insulating layer with zero conductivity can be derived so that it can reveal the dependence on the insulating layer properties:

$$M_n = 20 \log \left| 1 - \Gamma_N \left[ \cos \left( 4\pi \frac{e_n}{\lambda_n} \right) + j \sin \left( 4\pi \frac{e_n}{\lambda_n} \right) \right] \right| \tag{9}$$

with  $c$  as the celerity,  $e_n$  as the insulating layer thickness, and  $\lambda$  as the wavelength inside the insulating layer  $n$  affected by the relative dielectric permittivity  $\epsilon_{rn}$ . The reflection coefficient  $\Gamma_N$  from Equation (9) represents the product of the reflections occurring on the boundaries for any layer  $N$ , as it does in Equation (7). Having an overall knowledge of all the different mechanisms degrading or contributing to the shielding effectiveness, we can

generally express the total SE for a multilayer screen composed of an alternation between conductor and insulating layers:

$$SE_{N \text{ layers}} = \underbrace{\sum_{N=1}^{N_{max}} (SE_{2N-1})}_{\text{Conducting layers shielding}} + \underbrace{\sum_{N=2}^{N_{max}-1} (M_{2N-2})}_{\text{Insulating layers losses}} . \quad (10)$$

From Equation (10), it clearly appears that insulating layers do not contribute to SE by themselves, since they are only related to losses. However, the key point leans on the space between the two conducting layers, hence providing a new reflection induced by the second conductive surface.

Since the analytical model contains all the intrinsic parameters of the materials, it gives us an opportunity to investigate parametrically different multilayer shielding designs. Thus, we are able to optimize thin shielding screen configurations, where absorption will no longer be the main contributor (contrary to usual thick and bulky enclosures).

### 3. Numerical Studies of a Planar Shielding Sheet

The results presented in the following sections were obtained from a 3D numerical analysis. Then, a comparison was made with the ones obtained from the previously introduced analytical model. Thorough simulation studies were performed using transmission line matrix time-domain solver available in CST Microwave Studio, a 3D electromagnetic simulation software, CST Studio Suite 2022, Dassault Systems, France [22]. This model considerably reduces the calculation time for thin sheets from a few micrometers used inside large models to a few centimeters. To be able to compare SE numerical calculations to the analytical evaluations, it is essential that the 3D models remain within the same theoretically ideal conditions. This means that the planar sheet must be orthogonal to the incident EM field propagation direction  $z$ , and its dimensions  $x$  and  $y$  must extend without boundaries, as presented in Figure 4.

#### 3.1. Parametric Studies on Multilayer Shielding

The first multilayer screen model consists of a double copper (Cu) layer screen of 6  $\mu\text{m}$  thickness each, with one insulating layer thickness referenced  $e_n$  inserted in between. We study the effect of the thickness on the SE by varying this parameter between 0  $\mu\text{m}$  and 100  $\mu\text{m}$ . The initial case of 0  $\mu\text{m}$  spacing represents a single 12  $\mu\text{m}$  thickness copper screen. Detailed 3D models are developed using CST for different values of  $e_n$  keeping a 25  $\mu\text{m}$  step. The corresponding results for the SE obtained after performing numerous calculations are presented in Figure 5.

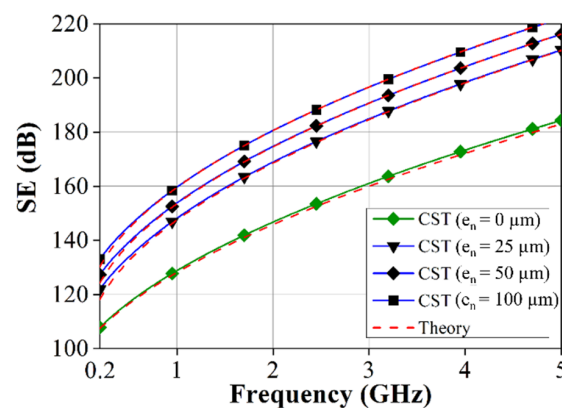


**Figure 5.** SE comparison between a 12  $\mu\text{m}$  Cu single layer (0  $\mu\text{m}$  spacing) and two 6  $\mu\text{m}$  Cu layers with a different spacing.

Furthermore, these results are compared with analytical ones and are discussed. The frequency was kept between 0.2 GHz and 5 GHz, respectively.

We can see here a good agreement between both methods along with the frequency range, which represents a valuable benefit of the developed numerical model. Additionally, an increase in SE is noticed between a single conducting layer and two spaced layers of the same total copper thickness.

The increase in SE is solely due to the shielding thickness increase. This is the reason why it is consistent to investigate the SE behavior when, for the same total thickness, the number of layers increases. We tested three specific configurations A, B, and C with an increasing number of layers: two, three, and four, respectively, for the same total screen thickness as presented in Table 1.

**Table 1.** Configurations of multilayer shielding screens with a same total thickness.

Configuration	Number of Copper Layers	Copper Layer Thickness $e_c$	Insulating Layer Thickness $e_n$
A	2	$2 \times 9 \mu\text{m}$	$1 \times 100 \mu\text{m}$
B	3	$3 \times 6 \mu\text{m}$	$2 \times 50 \mu\text{m}$
C	4	$4 \times 4.5 \mu\text{m}$	$3 \times 33 \mu\text{m}$

As observed in Figure 6, the benefits of moving from a single layer to a double layer regarding SE are obvious when subdividing the space into a higher number of layers (up to four). The obtained gain extends from 15 to 30 dB on most of the frequency window.

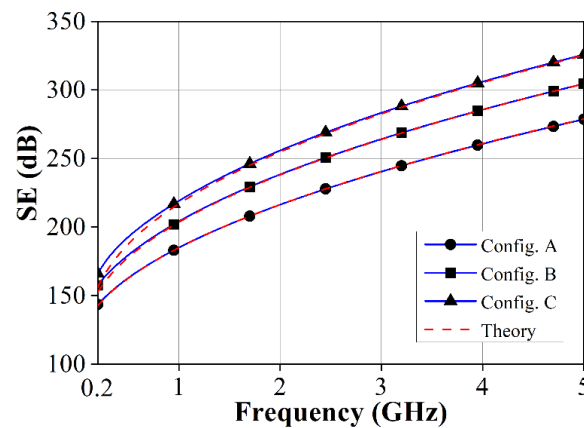


**Figure 6.** SE comparison between configurations A, B, C, obtained from simulation and from theory.

The multilayer designs shown in Table 1 and considered until now were built with insulating layers having the same thickness. However, it can be questioned if the total SE would be affected by introducing an asymmetry between these insulating layers, as represented at Figure 7. To investigate this, new three-layer shielding screen designs with an irregular distribution of the insulating layer’s thicknesses  $e_n$  are proposed and described in Table 2.

**Table 2.** Different asymmetry ratios between two insulating layers.

$\eta$	0.11	0.25	0.43	0.67	1	1.5	2.3	4	9
$e_{n2} (\mu\text{m})$	10	20	30	40	50	60	70	80	90
$e_{n4} (\mu\text{m})$	90	80	70	60	50	40	30	20	10

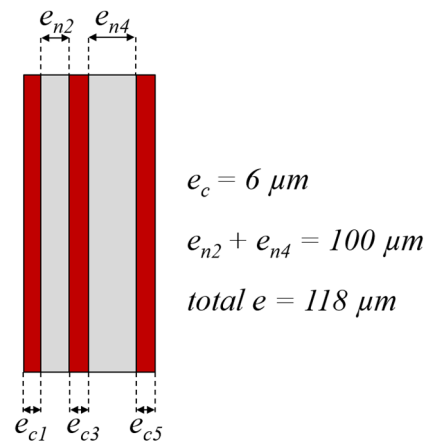


**Figure 7.** Three layers configuration (Cu-6 μm/Ins- $e_{n2}$ /Cu-6 μm/Ins- $e_{n4}$ /Cu-6 μm) with an asymmetry between insulating layers for the same total thickness of 100 μm.

These structures with different asymmetry ratios of  $\eta = e_{n2}/e_{n4}$  have been designed in the 3D model. SE simulations results are presented for a given frequency of 3 GHz and then compared with theoretical calculations obtained for the same design, as shown in Figure 8.

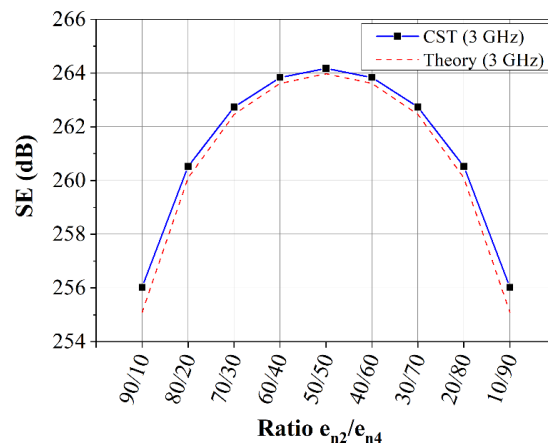


**Figure 8.** SE alteration for different asymmetry ratios at 3 GHz for 3 layers (Cu-6 μm/Ins- $e_{n2}$ /Cu-6 μm/Ins- $e_{n4}$ /Cu-6 μm) shielding screen.

In Figure 8, we can notice a decrease in SE as the ratio varies symmetrically on the frequency range to  $\eta \gg 1$  or  $\eta \ll 1$ . This change remains relatively weak—a few dB—compared to the whole SE level, but it should be considered for less effective shielding configurations with poor conductivity, as in [10]. It can be deduced from these results that the maximum SE will be obtained with perfect symmetry between insulating layers and that any asymmetry would only be detrimental.

### 3.2. The Case of High Permittivity Insulating Layers

The dielectric permittivity  $\epsilon$  of a non-conductive material is considered in both calculations of multiple reflection losses  $M_n$ , for a layer  $n$ , from Equation (9) and of its impedance  $Z_n = \sqrt{\mu_n/\epsilon_n}$ . In the case of a single layer,  $\epsilon$  depicts the environment around the shielding (which is air). The multilayer has its particularity since it allows for the opportunity to use insulating layers with dielectric permittivity different to air, as modeled in our SE calculations.

The periodicity of Equation (10) may be highlighted by calculating the modulus of  $M_n$  equal to:

$$M_n = |1 - \Gamma_N[\cos k + j \sin k]| = \sqrt{(1 - \Gamma_N \cos k)^2 + (\Gamma_N \sin k)^2} \tag{11}$$

where (see Equation (10)):

$$k = 4\pi \frac{e_n}{\lambda_n}. \tag{12}$$

Regarding frequency, the expression of  $k$  becomes:

$$k = 4\pi \frac{e_n \sqrt{\epsilon_{rn}}}{c} \times f. \tag{13}$$

The minimum modulus expressing maximum losses can be found for  $(k = \pi + 2\pi N)$  with  $N \in \mathbb{N}$ , and, therefore, at the following frequencies, which in fact are resonant frequencies:

$$f_0(N) = N \times \frac{c}{2e_n \sqrt{\epsilon_{rn}}}. \tag{14}$$

Simulations and analytical calculations have been performed for different values of  $\epsilon_{rn}$  varying from 1000 to  $2.5 \times 10^5$  applied to the 50  $\mu\text{m}$  thickness insulating layer of a double layer shielding screen (Cu-6  $\mu\text{m}$ /Insu.-50  $\mu\text{m}$ /Cu-6  $\mu\text{m}$ ), and the results are presented in Figure 9. Lower  $\epsilon_{rn}$  is irrelevant since the  $f_0$  would be very high above the gigahertz. The first peak ( $N = 1$ ) for  $\epsilon_{rn} = 10^5$  is found accordingly to Equation (14) at 9.5 GHz, and for  $\epsilon_{rn} = 2.5 \times 10^5$  at 6 GHz. It is also clear that besides the peaks, the total SE is decreased. This is due to the insulating layer impedance, which is different from the impedance in air or a vacuum and results in a lower reflection at the second conducting layer, since insulating and conducting layer impedances are closer in this configuration.

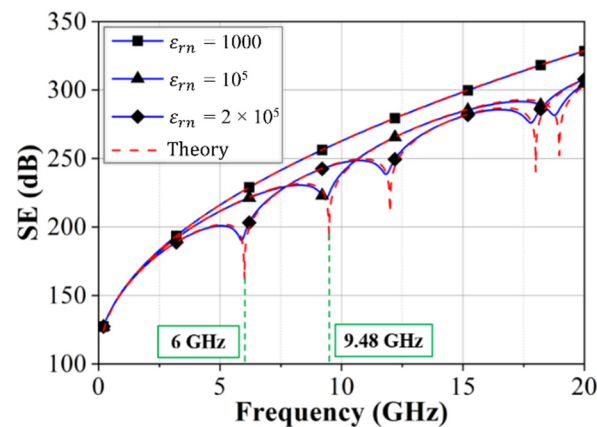


**Figure 9.** Comparison of SE with different dielectric permittivity levels for a double layer (Cu-6  $\mu\text{m}$ /Ins( $\epsilon_{rn}$ )-50  $\mu\text{m}$ /Cu-6  $\mu\text{m}$ ) shielding screen.

The high dielectric permittivity insulators inside multilayer shielding screens reduce reflection efficiency, in the frequency range of IEMI, 0.2–5 GHz, and thus reduce the total SE. The best performances are therefore obtained with an insulator transparent to EM waves, i.e., with similar properties than air.

#### 4. Simulations of the Shielding Enclosure Effectiveness with IEMI Aggression

This section discusses the SE consistency when a more real EM illumination scenario is considered. Firstly, the shielding screen is considered as a rectangular enclosure protecting a printed circuit board (PCB) instead of a perfect metallic plan as considered previously. Secondly, the EM source is differenced from an ideal plane wave, with the modelling of a dipole antenna located at a certain distance from the shielding Subject. While this scenario is too complex to apply the transmission line theory model, the use of the 3D numerical analysis represents a relevant approach to study these phenomena. The following numerical studies were performed using a transient co-simulation between the MW and Design Studio modules of CST.

#### 4.1. Design of the Subject 3D Model

Our chosen subject model presented in Figure 10 consists of a PCB protected with a Board Level Shielding (BLS) type enclosure [23], being typically applied in a specific area of the PCB where strong EM immunity is required to ensure full functionality of the system. In this study, the sensitive parts of our 250 MS/s ADC board developed for embedded data acquisition are the clock source components, which involve a voltage controlled oscillator (VCO) and a clock divider, which is consequently implemented in our 3D model (see Figure 10).

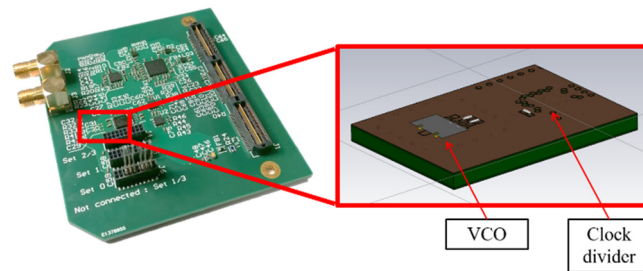


Figure 10. Analog to digital conversion PCB with 250 MHz clock generation area used as a 3D model.

As shown in Figure 11, the PCB sample is confined from both sides in a fully sealed metallic  $16 \times 22 \times 12 \text{ mm}^3$  enclosure. The composition of the shield is either a  $100 \mu\text{m}$  thickness of FR-4 material (non-conductive) where a single layer of  $12 \mu\text{m}$  (Cu) coating film on one side, or with  $6 \mu\text{m}$  (Cu) coating films applied on both sides of the FR-4 layer (double layer shielding). These two configurations are shown in Table 3.

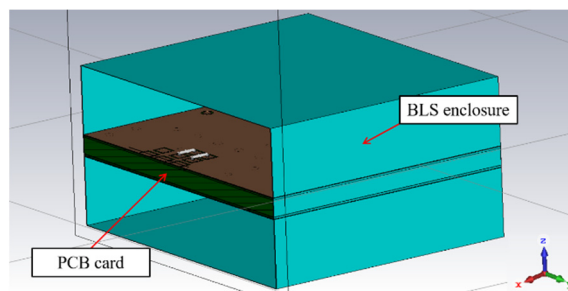


Figure 11. Sectional view of the PCB card shielded with a BLS type enclosure 3D model.

Table 3. Different BLS enclosure shielding compositions.

Configuration	Layer 1	Layer 2	Layer 3
A (single layer)	Cu- $12 \mu\text{m}$	FR4- $100 \mu\text{m}$	-
B (double layer)	Cu- $6 \mu\text{m}$	FR4- $100 \mu\text{m}$	Cu- $6 \mu\text{m}$

#### 4.2. Design of the EM Source 3D Model

To generate an EMI, a radiating source is defined as an antenna and inserted in the 3D model. Since the volume is a critical parameter for simulation time, the half-wave dipole antenna has been chosen as the EM source (Figure 12). Its well-known design allows us to accurately control parameters such as center frequency, bandwidth of the EM field, and  $E$ -field or  $H$ -field strength at a certain distance [24]. The band ratio ( $b_r$ ) of an antenna expressing its frequency bandwidth is defined as  $b_r = (f_h/f_l)$ , where  $f_h$  and  $f_l$  are high and low  $-3 \text{ dB}$  cut-off frequencies of the frequency spectrum, respectively. The  $b_r$  of a half-wave dipole antenna is found between 1.1 and 1.3, which can be considered, based on Figure 1, as a mesoband type spectrum of IEMI [8]. With the aim of covering the whole frequency spectrum of IEMI, ten designs and formats of antenna have been tested from

0.5 to 5 GHz. Their dimensions (gap distance  $G$ , diameter  $D$ , and length  $L$ ) were optimized for each center frequency following the classic design rules from [24].

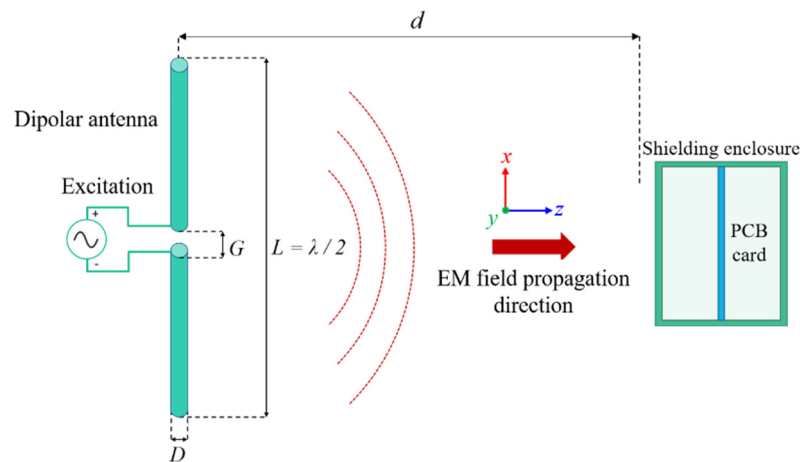


**Figure 12.** Schematic drawing of half-wave dipole antenna radiation.

To be able to reproduce the same aggression radiation condition as in our previous part, the antenna had to be placed at a distance  $d_f$  from the subject, where the incident EM field can be considered as far field. In addition, the antenna is oriented such that the EM field propagation direction is normal to the exposed face of the shielding enclosure. From an EM wave propagation point of view, the EM field is supposedly coupled for a distance  $d_f = (2L^2/\lambda)$ , also called Fraunhofer zone, where  $L$  is the length of the antenna and  $\lambda$  the wavelength of radiated EM field. In the case of a half-wave dipole antenna, the relation  $L = \lambda/2$ , means that the far field distance  $d_f$  is equal to  $\lambda/2$ . This ensures us in the meantime to be above and in compliance with the far field distance of  $\lambda/2\pi$  from the EM wave impedance point of view.

Therefore, the distance between the source and the subject has been fixed at twice  $d_f$ , which is equal to  $\lambda$ . This is a good compromise between ensuring far field conditions and ensuring a reasonable calculation time.

For a half-wave dipolar antenna,  $E$ -field in far field can be estimated as a function of distance:

$$E = \frac{\sqrt{1.64P}\sqrt{Z_0}}{2\sqrt{\pi}d} \approx 7\frac{\sqrt{P}}{d} \quad (15)$$

where  $E$  is the electric field in V/m,  $P$  the antenna radiated power in W,  $Z_0$  the impedance of EM field in air in  $\Omega$ . From literature, the linear gain of a half-wave dipole antenna was established to 1.64 [24].

According to EM immunity of the subject, this relation is important to specify the location of the system away from a certain source, and, as a consequence, the maximum endurable radiating power at a fixed distance. The  $E$ -field radiated from a 3 GHz antenna was simulated and is shown in Figure 13. Its maximum amplitude through distance obtained from the simulation was compared with the estimation from Equation (15).

As we can notice, both results fit very closely at the distance  $d = \lambda$ . Additionally, the divergence in near field since the  $E$ -field appears to decrease for  $1/d^2$  in this area.

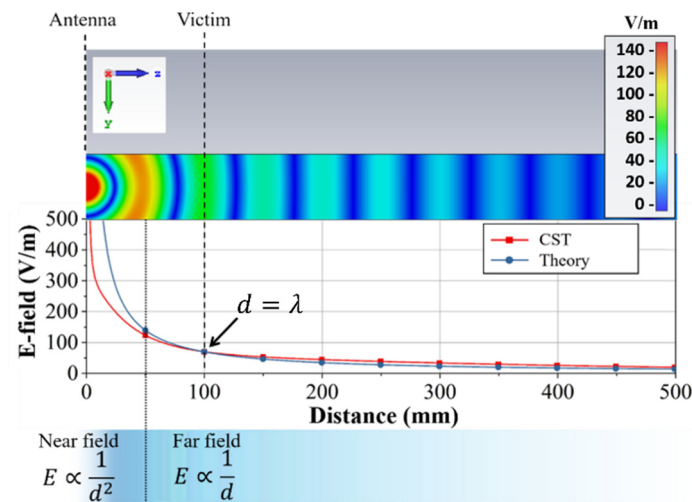


**Figure 13.** Simulation of  $E$ -field radiation from a 3 GHz half-wave antenna compared with theoretical  $E$ -field strength estimation in far field, in particular at the distance  $d = \lambda$ , where the subject is placed.

#### 4.3. Numerical Studies of the Cases of Susceptibility

Based on existing IEMI sources, the excitation pulse feeding the antenna was fixed to a 1 MV voltage amplitude [25]. This value is not critical since the study is focused on the shielding effectiveness, whose value according to Equation (1) is relative. It is, however, interesting for further studies, particularly for EMC purposes, to be able to relate  $E$ -field at a certain location around the board in correlation with the radiating source parameters. The whole 3D model (including the shielding enclosure and the IEMI source) was used to perform several simulations in order to estimate the shielding effectiveness of different enclosure designs. Figure 14 represents the numerical evaluation of the  $E$ -field inside the enclosure with two configurations. Figure 14a shows these numerical calculations in the case where no shielding is used. Figure 14b represents the  $E$ -field amplitude with the presence of a single layer shielding of Cu-12  $\mu\text{m}$ , constituting the shielding configuration A (see Table 3).

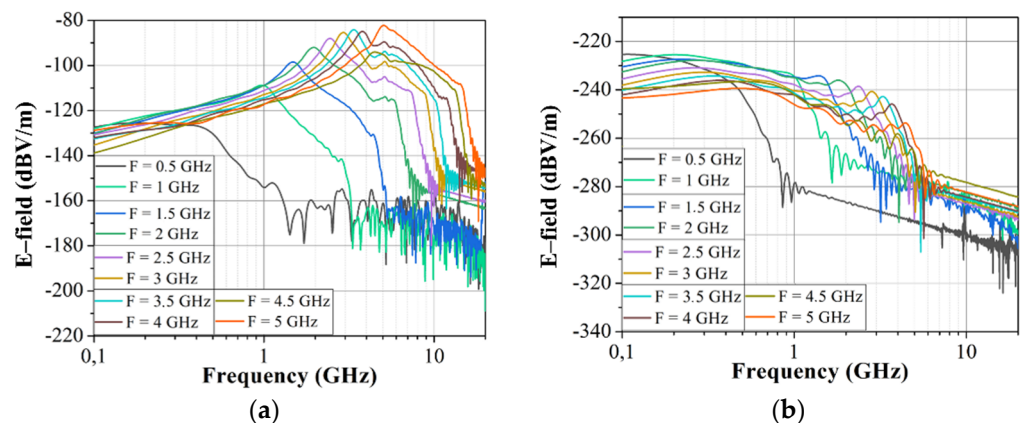


**Figure 14.** (a) Frequency spectrum of  $E$ -field measured near PCB without shielding. (b) Frequency spectrum of  $E$ -field measured with single 6  $\mu\text{m}$ -Cu layer shielding enclosure. Measurements are presented for the 10 half-wave dipolar antennas.

The ten curves show the  $E$ -field for each antenna central frequency, which have been placed respectively to a distance  $d = \lambda$ . As an example, the antenna with a central frequency of 0.5 GHz was placed at 60 cm from the enclosure, and the one with a central frequency of 5 GHz was placed at 6 cm. They are both considered to be in far field regarding to their respective central frequencies.

The  $E$ -field difference expressed in dB for each of the ten central frequencies from 0.5 GHz to 5 GHz was used to reconstitute the SE on the whole discrete frequency range. This process was applied for simulation results obtained with both configurations from Table 3: the single layer Cu-12  $\mu\text{m}$  configuration A, and the two conducting layers Cu-6  $\mu\text{m}$ /FR4-100  $\mu\text{m}$ /Cu-6  $\mu\text{m}$  configuration B (see Figure 15). The calculated SE was then compared to the ideal model results presented previously, and to the theoretical calculations.

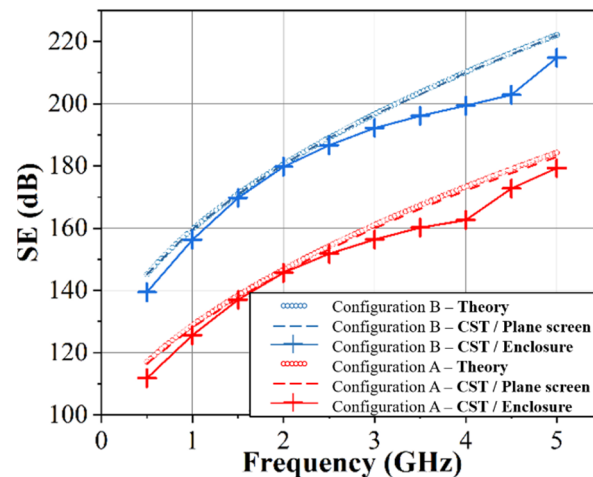


**Figure 15.** Comparison of SE obtained from simulation between theory, the CST plane screen, and the CST finite enclosure (configurations A and B).

We can observe an improvement from 30 to 40 dB between configurations A and B, which confirms the advantage of multilayer shieldings over single layer ones. Despite the appearance of a drop in SE around 4 GHz (which is common to both configurations), it is difficult to assume a relationship with cavity resonance modes of an enclosure of such size ( $22 \times 16 \times 11 \text{ mm}^3$ ), which is expected above 10 GHz.

## 5. Conclusions

The study presented in this article corroborates the advantages of multilayer shielding screens against single layer models by comparing the transmission line analytical model and the 3D EM numerical model. Different layer arrangements were investigated by isolating each parameter, thus allowing us to point out the effects on the shielding effectiveness in each case. It appears that the spacing increase between two conducting layers enhances the total SE by reducing multiple internal reflection losses that occur between them. In addition, the increase in layers number for the same total screen thickness helps to improve SE by multiplying the reflection coefficient by the number of conducting layers. The optimal SE is found by both analytical and numerical methods when the insulating layers have the same thickness. A gradient of these thicknesses would not allow any gain but would only decrease SE. It was also observed that a high enough relative permittivity ( $\epsilon_r > 10^4 \sim 10^5$ ) for thin insulating layers around 100  $\mu\text{m}$  thickness can bring resonant frequencies below 10 GHz and decrease the total SE. The overall results shown in this paper emphasize the gain in compactness of multilayer shielding over single layer classical shields. To reduce volume while keeping the same shielding effectiveness is fully in line with the continuous improvement for smaller, faster, and more EM sensitive embedded electronic systems operating in EMI environments.

Our study has also presented the development of a 3D co-simulation model, which includes all at once the subject and the source geometries. Thus, the ability to estimate SE with more complex and realistic 3D models will enhance the interest in studies dedicated to advanced shielding designs for significant EMC improvements. In further steps, it will give the possibility to estimate parasitic voltage disturbances induced in high-speed PCB tracks (clocks, data signals), and therefore, to anticipate maximum admissible EM field values for

safe operation of the target/subject. The two conditions for this (minimum distances to the source and maximum amplitude of sources power) could be settled for keeping good signal integrity and proper functioning of the fully shielded system.

## 6. Future Work

The experimental validation of such shielding is a well-known challenge, which cannot be easily met without the use of very specific equipment. In collaboration with CEA Gramat, the implementation of test campaigns in anechoic chambers, with the provision of IEMI type radiating sources, will be planned. This partnership will also allow us to project ourselves towards applications for board level shielding on actual monitoring devices. Moreover, as a completion of the study, the numerical analysis of shielding's behavior in near field, using our 3D models, is planned to be performed. Near field shielding theory is applicable to multilayer, though it can be challenging when it comes to analyzing it numerically or experimentally. Considering this important scenario for subject shielding, as well as emission shielding, would greatly enhance the radiated immunity behavior accuracy of future electric systems during their EMC design process.

**Author Contributions:** Conceptualization, R.L., N.I., R.R. and J.-M.D.; methodology, R.L., J.-M.D. and N.I.; software, R.L. and N.I.; supervision, R.R. and J.-M.D.; validation, R.R., J.-M.D., N.I. and V.G.; writing—original draft preparation, R.L. and N.I.; writing—review and editing, R.L., N.I., R.R., J.-M.D., N.I. and V.G. All authors have read and agreed to the published version of the manuscript.

**Funding:** This work was supported by the 'Commissariat à l'Énergie Atomique et aux Énergies Alternatives (CEA) CESTA', Cestas, France.

**Data Availability Statement:** Data is contained within the article. The data presented in this study are available in this paper.

**Conflicts of Interest:** The authors declare no conflict of interest.

## References

1. Yao, J.; Li, Y.; Wang, S.; Huang, X.; Lyu, X. Modeling and Reduction of Radiated EMI in a GaN IC-Based Active Clamp Flyback Adapter. *IEEE Trans. Power Electron.* **2021**, *36*, 5440–5449. [[CrossRef](#)]
2. Huang, H.-Y.; Villaruz, H.M.; Mapula, N.M. High-Efficiency Low-EMI Buck Converter Using Multistep PWL and PVT Insensitive Oscillator. *IEEE Trans. Power Electron.* **2022**, *37*, 9325–9332. [[CrossRef](#)]
3. Ji, S.; Zhang, Z.; Wang, F. Overview of high voltage sic power semiconductor devices: Development and application. *CES Trans. Electr. Mach. Syst.* **2017**, *1*, 254–264. [[CrossRef](#)]
4. She, X.; Huang, A.Q.; Lucia, O.; Ozpineci, B. Review of Silicon Carbide Power Devices and Their Applications. *IEEE Trans. Ind. Electron.* **2017**, *64*, 8193–8205. [[CrossRef](#)]
5. Giri, D.; Tesche, F. Classification of Intentional Electromagnetic Environments (IEME). *IEEE Trans. Electromagn. Compat.* **2004**, *46*, 322–328. [[CrossRef](#)]
6. Fujii, K.; Noto, Y.; Oshima, M.; Okuma, Y. 1-MW Solar Power Inverter with Boost Converter Using all SiC Power Module. In Proceedings of the EPE-ECCE Europe, Geneva, Switzerland, 8–10 September 2015; pp. 1–10.
7. Ozdemir, S.; Acar, F.; Selamogullari, U.S. Comparison of silicon carbide MOSFET and IGBT based electric vehicle traction inverters. In Proceedings of the ICEEL, Denpasar, Indonesia, 10–11 August 2015; pp. 1–4. [[CrossRef](#)]
8. Mishima, T.; Morinaga, S.; Nakaoka, M. All-SiC Power Module Applied Single-Stage ZVS-PWM AC–AC Converter for High-Frequency Induction Heating. In Proceedings of the IEEE IECON, Yokohama, Japan, 9–12 November 2015; pp. 004211–004216.
9. Sonnemann, F.; Bohl, J.; Ehlen, T. Comparison of Threshold and Destruction Levels at a Generic Electronic Device irradiated with UWB and NNEMP Pulses. In Proceedings of the EuroEM 2000, Edinburgh, Scotland, 30 May–2 June 2000.
10. Schulz, R.; Plantz, V.; Brush, D. Shielding theory and practice. *IEEE Trans. Electromagn. Compat.* **1988**, *30*, 187–201. [[CrossRef](#)]
11. Vance, E.; Graf, W. The role of shielding in interference control. *IEEE Trans. Electromagn. Compat.* **1988**, *30*, 294–297. [[CrossRef](#)]
12. Graf, W.; Vance, E. Shielding effectiveness and electromagnetic protection. *IEEE Trans. Electromagn. Compat.* **1988**, *30*, 289–293. [[CrossRef](#)]
13. Amato, T.; Mis, D.J.; Willard, B. Shielding effectiveness before and after the effects of environmental stress on metalized plastics. *IEEE Trans. Electromagn. Compat.* **1988**, *30*, 312–325. [[CrossRef](#)]
14. Ashtari, R.; Jones, D.H. Low-Frequency Magnetic Shielding. In Proceedings of the IEEE EMC SIPI, New Orleans, LO, USA, 22–26 July 2019; pp. 84–89.
15. Liu, Q.-F.; Ni, X.; Zhang, H.-Q.; Yin, W.-Y. Lumped-Network FDTD Method for Simulating Transient Responses of RF Amplifiers Excited by Intentional Electromagnetic Interference Signals. *IEEE Trans. Electromagn. Compat.* **2021**, *63*, 1512–1521. [[CrossRef](#)]

16. Watanabe, A.O.; Raj, P.M.; Wong, D.; Mullapudi, R.; Tummala, R. Multilayered Electromagnetic Interference Shielding Structures for Suppressing Magnetic Field Coupling. *J. Electron. Mater.* **2018**, *47*, 5243–5250. [[CrossRef](#)]
17. Gaoui, B.; Hadjadj, A.; Kious, M. Enhancement of the shielding effectiveness of multilayer materials by gradient thickness in the stacked layers. *J. Mater. Sci. Mater. Electron.* **2017**, *28*, 11292–11299. [[CrossRef](#)]
18. Merizgui, T.; Hadjadj, A.; Kious, M.; Gaoui, B. Comparison Electromagnetic Shielding Effectiveness Between Smart Multilayer Arrangement Shields. In Proceedings of the ICASS, Medea, Algeria, 24–25 November 2018.
19. Leduc, R.; Ruscassie, R.; Larbaig, J.M.; Courtois, L.; Dienot, J.M.; Reess, T. High Frequency Signals Synchronization using FPGA-SoC technology for security system in a radiography equipment. In Proceedings of the EAPPC-BEAMS-MEGAGAUSS'2021, Biarritz, France, 29 August–2 September 2021; p. 122.
20. Sun, X.; Wei, B.; Li, Y.; Yang, J. A New Model for Analysis of the Shielding Effectiveness of Multilayer Infinite Metal Meshes in a Wide Frequency Range. *IEEE Trans. Electromagn. Compat.* **2022**, *64*, 102–110. [[CrossRef](#)]
21. Ott, H. *Electromagnetic Compatibility Engineering*; Wiley: Hoboken, NJ, USA, 2011.
22. Computer Simulation Technology. Available online: <https://www.3ds.com/> (accessed on 27 March 2022).
23. Liu, Y.; He, R.; Khilkevich, V.; Dixon, P. Shielding Effectiveness of Board Level Shields with Absorbing Materials. In Proceedings of the IEEE EMC—SIPI, New Orleans, LO, USA, 22–26 July 2019; pp. 84–89. [[CrossRef](#)]
24. Stutzman, W. *Antenna Theory and Design*; Wiley: New York, NY, USA, 1998.
25. Baum, C.E.; Baker, W.L.; Prather, W.D.; Lehr, J.M.; O'Loughlin, J.P.; Giri, D.V.; Smith, I.D.; Altes, R.; Fockler, J.; McLemore, D.M.; et al. JOLT: A highly directive, very intensive, impulse-like radiator. *Proc. IEEE* **2004**, *92*, 1092–1109. [[CrossRef](#)]